

Decoherence Effects in Reactive Scattering

Heekyung Han and Paul Brumer

Chemical Physics Theory Group,

Department of Chemistry,

and Center for Quantum Information and Quantum Control,

University of Toronto

Toronto, Canada M5S 3H6

(Dated: November 29, 2018)

Abstract

Decoherence effects on quantum and classical dynamics in reactive scattering are examined using a Caldeira-Leggett type model. Through a study of dynamics of the collinear $\text{H} + \text{H}_2$ reaction and the transmission over simple one-dimensional barrier potentials, we show that decoherence leads to improved agreement between quantum and classical reaction and transmission probabilities, primarily by increasing the energy dispersion in a well defined way. Increased potential nonlinearity is seen to require larger decoherence in order to attain comparable quantum-classical agreement.

I. INTRODUCTION

Isolated molecular collisions have been the subject of theoretical study over the past half century. Amongst the successful tools in the field are classical trajectory approaches, whose justification often relies upon the relatively small deBroglie wavelengths in a chemical reaction. However, most chemical reactions occur in the condensed phase. Such an environment, due to its randomness, tends to decohere[1] a quantum system, driving it towards the classical limit. Hence, we would anticipate that the utility of classical methods would gain further validity from this loss of phase information. In this paper we investigate the extent to which quantum effects are lost, in chemical reactions, due to the environment. Specifically, we examine, using a Caldeira-Leggett type of approach [2, 3, 4] applied to the paradigmatic collinear H + H₂ system [5], the effects of the environment on the two predominant quantum effects in reactive scattering: tunneling and resonances. We find, for reasonable values of the decoherence, that the quantum dynamics of the (system + environment) approaches that of the classical dynamics of the (system + environment). A detailed analysis of the tunneling and resonance regimes is also provided through a study of simple one dimensional models. Improved decoherence-induced quantum-classical agreement in the reactive cross section is found, in both the tunneling and resonance regions, to stem from increasing energy dispersion with increasing decoherence strength and increasing interaction time.

The general issue of the transition from quantum to classical dynamics remains a subject of considerable interest and activity. Traditionally, classicality is argued to emerge as \hbar goes to zero or equivalently as the system mass goes to infinity. A comprehensive Liouville-based approach [6] provides a more complete description of this limiting process for both integrable and chaotic systems. Alternatively, decoherence, i.e. , the loss of quantum coherence as induced by the interaction of a system with its environment, has been proposed to be an essential ingredient for the utility of classical mechanics in the real world [1]. Early theoretical studies on model systems successfully demonstrated that decoherence is effective in bringing about classical behavior in the macroscopic limit [7]. In addition, our earlier study[8] extended this work to Hamiltonian systems, showing the emergence of classical behavior due to decoherence in a bound Hamiltonian system.

Despite numerous papers, and some applications in chemistry [9, 10] little work has been done on the role of decoherence in inducing classicality in scattering problems, such as

chemical reactions. We do so below, via a simple master equation for the reduced density matrix ρ , i.e. the density matrix for the scattering system after averaging over the external bath. The essential observable under consideration is the reactive scattering cross section, which displays both quantum tunneling and resonance scattering.

II. DECOHERENCE: FORMULATION AND COMPUTATION

Consider a scattering event that occurs in the presence of an external environment, focusing attention on the short time regime wherein decoherence, but not energy transfer between the system and environment, occurs. A master equation for ρ for such a setup has been obtained by Joos and Zeh [2] for an isotropic environment that elastically scatters from the system of interest with negligible momentum transfer. With the additional assumption that the $\langle x|\rho|x' \rangle$ of interest are those with $k|x - x'| \ll 1$, where k is the typical wavenumber of the environment and x is the system coordinate, they obtained an equation for ρ that is the same as the oft-cited model of Caldeira and Leggett [3] and that of Unruh and Zurek [4], when dissipation is ignored. The latter corresponds to ignoring the transfer of momentum to the environment, a reasonable assumption for the short time scales associated with the collision process.

For a system with two degrees of freedom, the resultant quantum master equation is given as [3, 12]:

$$\frac{\partial \rho}{\partial t} = \frac{1}{i\hbar}[H, \rho] - \frac{D}{\hbar^2}[x, [x, \rho]] - \frac{D}{\hbar^2}[y, [y, \rho]] \quad (1)$$

with the system Hamiltonian H and the decoherence constant D . To compare to the classical result it is convenient to consider this equation in the Wigner representation [3]:

$$\frac{\partial}{\partial t} \rho^W = \mathcal{L}_{\text{cl}} \rho^W + \mathcal{L}_{\text{q}} \rho^W + \mathcal{L}_{\text{D}} \rho^W; \quad (2)$$

$$\mathcal{L}_{\text{cl}} \equiv \{H, \cdot\}_{\text{PB}}, \quad (3)$$

$$\mathcal{L}_{\text{q}} \equiv \sum_{(l_1+l_2)=\text{odd}} \frac{1}{l_1! l_2!} \left(\frac{\hbar}{2i}\right)^{(l_1+l_2-1)} \frac{\partial^{(l_1+l_2)} V(x, y)}{\partial x^{l_1} \partial y^{l_2}} \frac{\partial^{(l_1+l_2)}}{\partial p_x^{l_1} \partial p_y^{l_2}}, \quad (4)$$

$$\mathcal{L}_{\text{D}} \equiv D \left(\frac{\partial^2}{\partial p_x^2} + \frac{\partial^2}{\partial p_y^2} \right). \quad (5)$$

where $\{\cdot\}_{\text{PB}}$ denotes the classical Poisson bracket and where $\rho^W \equiv \rho^W(p_x, p_y, x, y)$ denotes the Wigner transform of ρ . Here, The \mathcal{L}_{cl} generates the classical dynamics of the closed

system, and L_q generates the quantum corrections to this dynamics, whereas L_D induces decoherence in the open system. When $D = 0$ Eq. (2) becomes the quantum Liouville equation for the closed system.

Equation (2) is solved using the quantum state diffusion (QSD) approach [8, 13] wherein one solves an associated stochastic Schrodinger equation for the state vector given by

$$|d\psi\rangle = \left(-\frac{i}{\hbar}H - \sum_m \left[L_m - \langle L_m \rangle_{|\psi\rangle} \right]^2 \right) |\psi\rangle dt + \sum_m \left[L_m - \langle L_m \rangle_{|\psi\rangle} \right] |\psi\rangle dW_m. \quad (6)$$

Here the self-adjoint operators L_m represent the coupling between the system and environment, $\langle L_m \rangle_{|\psi\rangle} = \langle \psi | L_m | \psi \rangle / \langle \psi | \psi \rangle$, and W_m is a complex Wiener process [13]. Our specific implementation of the QSD method takes the operators L_m as $L_1 = \frac{\sqrt{D}}{\hbar} \hat{x}$ and $L_2 = \frac{\sqrt{D}}{\hbar} \hat{y}$. Computationally, the unitary component of Eq. (6) is integrated by the fast Fourier transform method plus the split-operator [14], as in a closed quantum system. The terms involving L_m are integrated using a second order scheme [15]. The dynamics resulting from the Stochastic Schrödinger equation (6), when averaged over many realizations of the Wiener process, provides the solution to Eq. (2) [13]. Hence, the quantum reaction probabilities for the open system are obtained by averaging over reaction probabilities for each wavefunction.

A comparison of these results with the classical result means comparing the quantum result of the (system + environment) with the classical result for the (system + environment). The latter is obtained by setting $L_q = 0$ in Eq. (2), leading to the classical Fokker-Planck equation for the classical density $\rho^{\text{cl}} \equiv \rho^{\text{cl}}(p_x, p_y, x, y)$:

$$\frac{\partial}{\partial t} \rho^{\text{cl}} = L_{\text{cl}} \rho^{\text{cl}} + L_D \rho^{\text{cl}}. \quad (7)$$

The resultant dynamics is equivalent to the Langevin-Itô equations with Gaussian white noise for each degree of freedom, which are solved by combining Monte Carlo sampling from the initial distribution and fourth-order Runge-Kutta integration. Results in the absence of decoherence ($D = 0$) were obtained directly by solving Hamilton's equations for the classical trajectories. The classical reaction probabilities for both the closed and open cases are obtained by counting the number of trajectories that are reactive.

III. H + H₂

A. Computational Features

We present results for collinear H + H₂. Isotopic variants of this system were also studied [22], with similar results to those reported here. The Hamiltonian for the collinear H + H₂ system is $H = \frac{1}{2\mu}(p_x^2 + p_y^2) + V(x, y)$, where x and y are the mass-scaled Jacobi coordinates of R (the distance of H from the center of mass of H₂) and r (the H₂ internuclear distance), respectively, and p_x and p_y are the corresponding momentum operators. The reduced mass $\mu = \sqrt{[m_1 m_2 m_3 / (m_1 + m_2 + m_3)]}$ where m_i is the mass of H. The Liu-Siegbahn-Truhlar-Horowitz potential energy surface[16] was used for $V(x, y)$.

The initial wavefunction, placed far from the interaction region, can be written as the product of a minimum uncertainty Gaussian wave packet $F(x)$ describing the relative initial translational motion times the vibrational eigenfunction $\phi_v(y)$ for H₂ with vibrational quantum number v . That is, $\psi(x, y, t = 0) = F(x)\phi_v(y)$, with

$$F(x) = (2\pi\gamma^2)^{-1/4} \exp\left[-\frac{(x - x_0)^2}{4\gamma^2} - \frac{ip_{x0}x}{\hbar}\right]. \quad (8)$$

Here γ is the width of $F(x)$, and x_0 and p_{x0} describe the locations of the initial wavepacket in position and momentum, respectively. A large value of γ results in a spatially delocalized wavepacket that is localized in momentum space. The initial total energy, E , is a sum of the average kinetic energy of the translational wavepacket and the vibrational energy. In the study below we consider the ground vibrational state ($v = 0$) and vary the translational energy. Note that the energy width $\delta E \equiv \sqrt{\langle H^2 \rangle - \langle H \rangle^2}$ of the initial wavepacket, of considerable interest later below, is determined by the translational component. Thus, by choosing γ appropriately the wavepacket can be focused on one average energy component of interest, E , with a narrow energy width. Specifically, since the initial wavepacket is in the asymptotic region ($x \rightarrow \infty$) and p_{x0} is chosen as $p_{x0} = -\sqrt{2\mu(E - E_v)}$, δE is given by $\delta E = \sqrt{\frac{\hbar^4}{32\gamma^4\mu^2} + \frac{\hbar^2(E - E_v)}{2\gamma^2\mu}}$, with vibrational energy E_v . Since the smaller the γ , the faster the numerical computation, γ is taken as small as possible, limited by the need to obtain an adequate δE that depends on the resolution of energy region studied. Our choice of $\gamma=5.9$ a.u. gives a $\delta E \approx 0.068$ eV for the initial wavepacket, which is somewhat larger, due to computational limitations, than that expected analytically.

To examine quantum-classical correspondence requires an appropriate comparison with an initial classical ensemble corresponding to the above initial quantum state. For the translational component, this is given by the Wigner function corresponding to $F(x)$ in Eq. (8). However, there are several possible choices for the vibrational component, which can be used to make the initial quantum and classical conditions as similar as possible [17, 18, 19]. For example, since the initial state is a vibrational eigenfunction, the corresponding Wigner function does not vanish at the classical vibrational turning points, so that some phase points have initial classical energies that do not equal the quantized value. The resultant δE for the vibrational motion differ for the initial quantum and classical density functions; the vibrational energy width of the initial quantum state is zero but that of the classical density is $\hbar\omega/2$. For the case of H_2 , this equals 0.27 eV. This width is much larger than that of the quantum counterpart whose entire energy width, 0.068 eV, comes from the translational part. This leads to classical reaction probabilities that are insensitive to decoherence.

Our results show that for studies of reaction probabilities versus energy, it is crucial to have the same initial δE for both the quantum and classical systems. Hence, each classical trajectory is chosen to have the fixed quantum vibrational energy, guaranteeing the same δE as that of the quantum system. We assume that H_2 is described as a Morse oscillator and obtain the initial vibrational variables as in Ref. [18, 20].

Below, two different values of D are examined. The smaller of the two, $D = 2.47 \times 10^{-35}$ kg·J/s, corresponds to 10^{-2} to 10^{-1} of typical D values in solution (a value estimated in Appendix). The larger D is 20 times the size of the smaller. Both these values of D are in the range extracted for D from a pseudo-realistic model problem [21]. For the open quantum system we averaged over 72 realizations for the smaller decoherence and over 288 realizations for the larger one. For both the closed and open classical systems 10^4 trajectories are used. Below, the notation QM and CM denote the quantum mechanical and classical probabilities, respectively, in the absence of decoherence. The symbols QMD and CMD denote results in the presence of decoherence.

We focus below on the effect of decoherence on the total reaction probability $P^R(E)$, which can be written as

$$P^R(E) = \int_0^\infty J^R(t, E) dt = \Delta t \sum_{n=0}^\infty J^R(n\Delta t, E), \quad (9)$$

with a chosen time increment Δt . Here the reaction flux, $J^R(t, E)$ is given as:

$$J^R(t, E) = (\hbar/\mu)\text{Im}[\langle\psi_E(x, y = y_I, t)|\partial\psi_E(x, y = y_I, t)/\partial y\rangle], \quad (10)$$

where $\psi_E(x, y, t)$ is the system wavefunction at time t that evolves from an initial wavepacket $\psi_E(x, y, t = 0)$ that is very narrowly focused on E , and the brackets denote the integration over x , obtained by adding all the discrete contributions over the entire range of x along a dividing line $y = y_I$ in the product region.

The simulation uses absorbing boundary conditions that damp the wave packet with a sine masking function near the edge of the grid in both reactant and product channels [23]. We used the following parameters for QM and QMD; the grid starts at $(x, y) = (x_{\min}, y_{\min}) = (0.90, 0.38)$, the mesh size $(\Delta x, \Delta y) = (0.15, 0.12)$, the initial position $(x_0, y_0) = (30, 1.35)$, and $y_I = 3.02$ in atomic units. For QM, $\Delta t = 0.14$ fs, and for QMD Δt is 0.073 fs for the smaller D and 0.012 fs for the larger D . The total time steps are chosen appropriately, keeping $t_f = 287$ fs constant. The classical reaction probability is evaluated by counting the number of trajectories that cross the dividing line $y = y_I^{\text{CM}} = 5$ a.u. before the final time $t_f^{\text{CM}} = 290$ fs. Numerical checks of quantum and classical calculations simulations at different temporal and spatial resolutions were carried out, and results for the closed systems were checked against previously computations [17, 18, 19].

B. Computational Results

Figures 1 and 2 display the classical and quantum reaction probabilities as a function of E for the H + H₂ exchange reaction in the closed system and open systems for both values of D . For the closed system the results agree well with those of the previous studies [18] and one sees large deviations between the classical and quantum probabilities. In particular, note the strong quantum resonance dips at $E \sim 0.9$ eV $E \sim 1.2$ eV as well as the tunneling that are all absent in the classical result. Upon introducing the smaller of the decoherence, the resonances are damped out, as seen in Fig. 1, leading to better agreement between quantum and classical reaction probabilities. Also notable is that the addition of the decoherence in Fig. 1 enhances the reaction probabilities at $E < 0.55$ eV and suppresses them at 0.55 eV $< E < 0.7$ eV, for both the quantum and classical cases. This behavior is even more pronounced in the case of the larger D , shown in Fig. 2, and is analyzed in Section V B where

tunneling in one dimension is examined in detail. Note from Fig. 1 that the CMD and QMD results are still in considerable disagreement. This disagreement disappears with the higher D [Fig. 2] where the classical and the quantum results are in very good agreement over the entire energy region. However, in this case most of the scattering structure is suppressed: the reaction probabilities are elevated at energies below the threshold and reduced above the threshold energy, and the P_R curve is now only slightly convex about $P_R = 0.5$.

Note that we also examined the case where the Wigner function is used for the vibrational component of the initial classical ensemble. In this case the classical reaction probabilities showed, in the threshold region, a slower rise with energy than the quantum counterparts in both the closed and open systems. This behavior is due to the larger δE of the initial classical density. In this case the resultant insensitivity of the classical reaction probabilities to decoherence leads to a persistent discrepancy between quantum and classical reaction probabilities, especially in the threshold region. Hence, in this case, basing the classical density on the Wigner function provides misleading results.

Having demonstrated that classical dynamics emerges in the presence of decoherence for the $\text{H} + \text{H}_2$ reaction, it remains necessary to identify the specific mechanism by which this occurs in the Caldeira-Leggett type model. To do so, we first show below that the system energy dispersion $\delta E = [\langle H^2 \rangle - \langle H \rangle^2]^{1/2}$ increases in these models as \sqrt{D}/m . Tunneling and resonance behavior for a simpler one dimensional model are then examined to establish the role of this increasing δE as the source of the decoherence-induced quantum-classical correspondence. We then return to remark on the case of reactive $\text{H} + \text{H}_2$.

IV. TIME EVOLUTION OF THE ENERGY DISPERSION δE

The friction free version of the Caldeira-Leggett master equation [Eq. (1)] is known to display an increase in system energy due to the D dependent decoherence term (the so-called environmental localization term). This energy increase would be compensated for, at far longer times, by the transfer of energy back to the environment [12]. More significantly, for our purposes, is the fact, shown below, that over similar timescales the square of the energy dispersion $(\delta E)^2 = \langle H^2 \rangle - \langle H \rangle^2$ increases as D/m^2 , where m is the system mass. To see this, we extend the method of Ref. [12] to the case of energy dispersion.

For simplicity, consider a one dimensional case, in which Eq. (1) reduces to

$$\frac{\partial \rho}{\partial t} = \frac{1}{i\hbar} [H, \rho] - \frac{D}{\hbar^2} [x, [x, \rho]]. \quad (11)$$

For any observable O that does not have explicit time dependence:

$$\begin{aligned} \frac{d\langle O \rangle}{dt} &= \frac{d}{dt} \text{Tr}(O\rho) \\ &= \text{Tr} \left(O \frac{\partial \rho}{\partial t} \right) \\ &= \frac{1}{i\hbar} \text{Tr} \left(O [H, \rho] \right) - \frac{D}{\hbar^2} \text{Tr} \left(O [x, [x, \rho]] \right). \end{aligned} \quad (12)$$

We note two useful relations: the cyclic invariance of the trace, which gives

$$\text{Tr}(A[B, C]) = \text{Tr}([A, B]C), \quad (13)$$

and the identity

$$[A, f(B)] = df/dB [A, B], \quad (14)$$

which holds when $[A, [A, B]] = [B, [A, B]] = 0$. Using Eqs. (13) and (14) one can verify the following relations:

$$\begin{aligned} \text{Tr}(x[x, [x, \rho]]) &= 0, \\ \text{Tr}(V(x)[x, [x, \rho]]) &= 0, \\ \text{Tr}(V^2(x)[x, [x, \rho]]) &= 0, \\ \text{Tr}(p_x[x, [x, \rho]]) &= 0, \\ \text{Tr}(p_x^2[x, [x, \rho]]) &= -2\hbar^2, \\ \text{Tr}(p_x^4[x, [x, \rho]]) &= -12\hbar^2 \langle p_x^2 \rangle, \\ \text{Tr} \left(\left\{ p_x^2 V(x) + V(x) p_x^2 \right\} [x, [x, \rho]] \right) &= -4\hbar^2 \langle V(x) \rangle. \end{aligned} \quad (15)$$

which are used to evaluate the effect of the environmental localization term.

Given these expressions the time-evolution of the energy dispersion can be evaluated. Specifically:

$$\begin{aligned} \frac{d(\delta E)^2}{dt} &= \frac{d\langle H^2 \rangle}{dt} - 2\langle H \rangle \frac{d\langle H \rangle}{dt} \\ &= D \left(3\langle p_x^2 \rangle / m^2 + 2\langle V(x) \rangle / m \right) - 2 \left(\langle p_x^2 \rangle / 2m + \langle V(x) \rangle \right) D / m \\ &= 2D \langle p_x^2 \rangle / m^2, \end{aligned} \quad (16)$$

where H is the system Hamiltonian given by $H = p_x^2/2m + V(x)$ and where we have used the result [12] that $d\langle H \rangle/dt = D/m$. The extension to the two-dimensional $H + H_2$ system is straightforward, giving

$$\frac{d(\delta E)^2}{dt} = \frac{2D}{\mu^2} \langle p_x^2 \rangle + \frac{2D}{\mu^2} \langle p_y^2 \rangle, \quad (17)$$

and the rate of the average energy increase becomes $4D/\mu$.

V. DECOHERENCE IN ONE DIMENSIONAL SCATTERING

A. Model Systems

As is well known [25], systems with increasing nonlinearity are expected to show increasing quantum contributions to the dynamics. Hence we consider the effect of decoherence on several one-dimensional barrier potentials of different nonlinearities. Two different types of barriers are designed for each degree of nonlinearity, a single barrier potential (denoted SB) showing no resonance and a double barrier potential (denoted DB) that shows a typical resonance in the transmission probability versus initial energy. The insights gained from these simple systems help shed light on the $H + H_2$ results.

For the one-dimensional cases, the computational formulae introduced above reduce to the analogous equations for one degree of freedom. The numerical methods used to obtain transmission probabilities in the quantum and classical systems are the same as described in the $H + H_2$ reaction case, the only difference being that here the absorbing potential at the grid boundary is not implemented. Instead, a sufficiently large position range is used so that the wavepacket does not encounter the boundary during the time evolution. The labels QM, CM, QMD and CMD have the same meaning here as described in the $H + H_2$ case. For the open quantum system a total of 500-1000 wavepackets are used, and for both the closed and open classical systems 10^4 trajectories are used. All variables below are in dimensionless units.

The Hamiltonian for one-dimensional scattering is

$$H = \frac{1}{2m} p_x^2 + V(x) = -\frac{\hbar^2}{2m} \frac{d^2}{dx^2} + V(x), \quad (18)$$

with mass m and potential $V(x)$. Here $m = 1$ and $\hbar = 0.1$. The initial wavefunction is chosen as a minimum uncertainty Gaussian wave packet $F(x)$ [Eq. (8)], and the associated Wigner function is used as the initial classical ensemble. In order to set δE of the initial wavepacket the same method as described above is used, except that here E_v is zero, and the mass and \hbar are different. We choose $p_{x0} = \langle p_x \rangle = \sqrt{2mE - \hbar^2/4\gamma^2}$, and thus $\delta E = \sqrt{-\frac{\hbar^4}{32\gamma^4 m^2} + \frac{\hbar^2 E}{2\gamma^2 m}}$. Specifically, we take

$$V_{\text{SB}}(x) = V_0[\cosh(\alpha x)]^{-2}, \quad (19)$$

$$V_{\text{DB}}(x) = V_{\text{SB}}(x - \beta) + V_{\text{SB}}(x + \beta) \quad (20)$$

as potentials for the SB case and for the DB case, respectively. The degree of system nonlinearity is estimated via a characteristic potential length, $\chi_n (\equiv |\partial_x V / \partial_x^{n+1} V|^{1/n})$ [25]: the smaller the χ_n , the larger the nonlinearity. Since the derivatives of these potentials obey the following relations:

$$d^{2n+1}V(x)/dx^{2n+1} = (-4\alpha^2)^n dV(x)/dx, \quad (21)$$

$$d^{2n}V(x)/dx^{2n} = (-4\alpha^2)^{n-1} dV^2(x)/dx^2, \quad (22)$$

$\chi_{2n+1} = 1/2\alpha$ for both the SB and DB cases. Hence, increasing α leads to the larger nonlinearity. For the SB case, we examine two cases, a weakly nonlinear potential (denoted SBW) and a strongly nonlinear one (denoted SBS) with $\alpha = 0.5$ and $\alpha = 10$, respectively. For the DB case, $\beta = 0.1$ and only a strongly nonlinear case with $\alpha = 10$ is examined. All V_0 are chosen to give the same barrier height of 2.0 and numerical parameters are chosen to ensure accuracy [26].

Figure 3 shows the potential energy for SBW, SBS, and DB along with their first derivatives. Since the nonlinearity is inversely proportional to the width of the potential energy, a narrow/wide barrier has a large/small nonlinearity. This can be clearly seen in Fig. 3. Thus, noting that the first derivatives of SBS and DB are approximately 20 times larger than that of SBW, we anticipate that the quantum corrections for SBS and DB should be comparable to one another and larger than that of SBW and that the magnitude of the decoherence needed for the emergence of classicality in the SBW case should be smaller than that of the SBS case. This is indeed observed below.

B. Tunneling Regime

Figure 4 shows the results of the tunneling calculations. For cases with no decoherence, in addition to the classical (CM) and quantum (QM) results, we show the exact quantum-mechanical transmission probabilities for the single barrier potentials, denoted QMA. They are given by [27]

$$P_R = \sinh^2(\pi p_{x0}/\hbar\alpha)/[\sinh^2(\pi p_{x0}/\hbar\alpha) + \cosh^2\{\pi/2\sqrt{c^2 - 1}\}] \quad (23)$$

where $c^2 \equiv 8mV_0/\hbar^2\alpha^2 > 1$, and used as a computational check. In the absence of decoherence the strongly nonlinear cases, SBS and DB, show larger differences between the quantum and classical results than does the weaker nonlinearity case. Further, tunneling in the quantum cases is clear, as is the broad resonance around $E = 2.6$ in the double barrier case, reflecting the presence of a metastable state in the quantum double barrier.

In Fig. 4, the decoherence shown is of magnitude that lead to roughly good agreement between quantum and classical results. In panel (a) this corresponds to $D = 6 \times 10^{-4}$, but in panels (b) and (c) the required $D = 3 \times 10^{-2}$, i.e. it is 50 times larger than that in (a). A comparison of results between the closed and open systems shows that introducing decoherence substantially improves quantum-classical correspondence. Several relevant observations are in order. First, the quantum resonance in the DB case is suppressed by increasing decoherence, leading to better agreement between quantum and classical transmission probabilities. This is discussed further in Section V C. Second, in order to reach classicality, the decoherence needed for both the SBS and DB cases is 50 times larger than that of the SBW case, due to the higher nonlinearity of their potentials. It is tempting to envision that classicality in the double barrier case might be reached with smaller decoherence than that of the single barrier SBS case of the same nonlinearity, since the quantum DB results shows a resonance that is absent in the SBS case. This view comes from the semiclassical picture [28] suggesting that the resonance region may be more sensitive to decoherence than is the threshold region since resonance require constructive interferences between trajectories. However, careful examination shows that it is the nonlinearity that dictates the magnitude of the decoherence required to reach classicality.

The third observation requires more attention. Note that Fig. 4 captures an overall qualitative picture of decoherence effects on the transmission probabilities. That is, in both the quantum and classical cases, decoherence enhances the transmission at energies below

the barrier height and suppresses it above the barrier height, similar to the trend seen in $H + H_2$. This behavior can be understood by considering the increase in energy width δE associated with introducing decoherence of the type given in Eq. (1). Figure 5 shows the computed growth of δE for the closed and open systems in the SBS case. The quantum and classical energy widths are seen to be in good agreement as a function of time, and become comparable to the 2-unit high barrier. Noting that the average energy $\langle E \rangle$ for the open system increases linearly with the rate of D/m [12] as well, one can understand from the classical point of view why decoherence enhances the transmission at $E = 1.4$, suppresses it at $E = 3.0$, and has little effect at $E = 2.0$ [Fig. 4(b)]. Specifically, at the collision time of $t \approx 3$, in the presence of decoherence, δE is approximately 1.05, 0.75, and 0.70 [Fig. 5] for the initial average energy $E = 3.0, 2.0$, and 1.4 , respectively, and is much larger than the average energy increase (≈ 0.06). Consequently, when the wavepacket of $E = 3.0$ strikes the barrier, the decoherence-induced δE increases that part of the wavepacket below the barrier height, increasing the reflected component, and reducing the transmission probability. (Note that although the average energy increases, decoherence-induced changes in the portion of the wavepacket above the barrier will not alter the transmission, since it will transmit in any case.) By contrast, for the case of $E = 1.4$, decoherence increases the portion of the energy above the barrier, allowing it to pass over the barrier, thus increasing the transmission probability. For the case of $E = 3.0$ and $E = 1.4$ the same trends are seen in both the quantum and classical results. On the other hand, for $E = 2$, equal to the barrier height, the transmission probability is rather insensitive to the decoherence. Similar observations apply to the other barrier cases.

C. Resonance Regime

Consider now the resonance region. This region has a characteristic width denoted δE_R . It is reasonable to assume that when D is sufficiently large to ensure that δE is on the order of δE_R at the time of the scattering resonance t_R then the resonance feature is eliminated. To obtain a crude estimate of the D for which this occurs consider Eq. (16):

$$\frac{d(\delta E)^2}{dt} = 2D\langle p_x^2 \rangle / m^2 \approx 4DE_0/m, \quad (24)$$

where E_0 is $\langle H \rangle$ at time zero. Here, in order to obtain a simple estimate, the initial kinetic energy has been assumed constant in time. Noting that here δE at time zero is ignorable compared to the growth rate, gives

$$\delta E = \sqrt{4DE_0t/m}. \quad (25)$$

A comparison with Fig. 5 shows that this drastic approximation simply replaces the saturation behavior by linear growth of δE , overestimating the growth of δE .

The simplest D estimate is then that the resonance width δE_R , which occurs at time t_R , will be washed out for decoherence strengths D_R on the order of:

$$D_R \approx (\delta E_R)^2 m / [4E_0 t_R] \quad (26)$$

Sample computations using this estimate are shown in Fig. 6 for the DB case with varying mass m (which implicitly changes δE_R and t_R). In the cases shown, δE_R varied from 0.6 to 0.3 and D_R from 0.007 to 0.0035. In all cases we compare the decoherence free result (denoted QM) to the result with either decoherence with D_R or, for comparison, with two different values of D , one being D_R . As is evident from Figure 6 the characteristic resonance shape disappears with the application of decoherence of magnitude D_R in each case. Interestingly, as in $H + H_2$, the resonance region disappears via a lowering of the initial peak that indicates resonant behavior, leaving a smooth falloff of P_R with decreasing energy. The smaller values of D , shown in panels (a) and (b) for comparison, are insufficiently large to completely eliminate the resonance.

D. $H + H_2$

This argument can be extended to the resonance region in $H + H_2$. Since our quantum $H + H_2$ calculation does not provide the increase of δE (due to absorbing boundary conditions), δE is estimated from the classical ensemble. At $t = 150$ fs $\sim t_f/2$ and at $E = 0.9$ eV, which is near the resonance dip, the smaller decoherence magnitude used above ($D = 2.47 \times 10^{-35}$ kg·J/s) gives an average energy increase of ~ 0.004 eV, which is relatively small compared to the average energy, and an energy width $\delta E \sim 0.08$ eV, which is roughly comparable to the resonance width. Hence, one would expect only partial elimination of the resonance, which is indeed the case [Fig. 1]. By comparison, the larger value of D used

[Fig. 2] is expected to have a δE that is roughly 0.4 eV and an average energy increase of ~ 0.09 eV, giving the extremely broad featureless results in Fig. 2. The resultant behavior in the $\text{H} + \text{H}_2$ case, is then entirely consistent with the broadening due to the decoherence induced δE .

VI. SUMMARY

Decoherence has been shown to significantly alter both the quantum and classical $\text{H} + \text{H}_2$ reaction probabilities, leading to quantum-classical agreement at realistic decoherence values. Unexpected behavior in the tunneling region, where the reaction probability is increased below the reaction threshold, but decreased above the threshold, lead to a more detailed examination of decoherence in the tunneling regime of simple one dimensional problems. The results of this study showed that (a) the extent of potential nonlinearity dictated the extent of decoherence required to reach quantum-classical agreement: that is, the larger the nonlinearity, the higher the required decoherence parameter, and (b) that the increase in energy width, due to environmental-induced localization, was responsible for the observed correspondence in probabilities in the tunneling and resonance regimes.

Studies of this type also made clear the general dearth of information on actual decoherence parameters for realistic systems. For this reason, realistic studies of this type are in progress [29].

Acknowledgments: We thank Dr. S. Mahapatra and Prof. N. Sathyamurthy for sharing a program code for the closed quantum system in the collinear $\text{H} + \text{H}_2$ reaction, and Dr. Jiangbin Gong for discussions. This work was supported by the Natural Sciences and Engineering Research Council of Canada and by Photonics Research Ontario.

Appendix: Values of D

Within Caldeira-Leggett type models, the constant D is related to the relaxation constant, f by [30]

$$D = 2fmkT, \tag{27}$$

where m is the system mass, k the Boltzmann constant, T the temperature of the environment, and f the strength of the system-environment coupling. Since a typical velocity relaxation time for small molecules is 0.01 - 0.1 ps [31], D_{typical} is roughly $10^{-33} - 10^{-34}$ kg·J/s for the mass of hydrogen at room temperature. This gives, for our choice of the smaller value of D that $D/D_{\text{typical}} \sim 10^{-2} - 10^{-1}$.

-
- [1] I. O. Stamatescu, E. Joos, H. D. Zeh, C. Kiefer, D. Giulini, and J. Kupsch, *Decoherence and the Appearance of a Classical World in Quantum Theory*, 2nd ed. (Springer Verlag, 2003); W. H. Zurek, Rev. Mod. Phys. **75**, 715 (2003); P. Blanchard, D. Giulini, E. Joos, C. Kiefer, I. O. Stamatescu (eds), *Decoherence: Theoretical, Experimental, and Conceptual Problems*, 2nd ed. (Lecture Notes in Physics 538, Springer Verlag, 2000).
- [2] E. Joos and H.D. Zeh Z. Phys. B 59, 223 (1985)
- [3] A.O. Caldeira and A.J. Leggett, Physica **121A**, 587 (1983).
- [4] W.G. Unruh and W.H. Zurek, Phys. Rev. D **40**, 1071 (1989); B.L. Hu, J.P. Paz and Y. Zhang, Phys. Rev.D **45**, 2843 (1992); **47**, 1576 (1993)
- [5] R. Sadeghi and R. T. Skodje, J. Chem. Phys. **99**, 5126 (1993) and references are therein.
- [6] J. Wilkie and P. Brumer. Phys. Rev. A 55, 27 (1997); *ibid.* Phys. Rev. A 55, 43 (1997).
- [7] S. Habib, K. Shizume, and W. H. Zurek, Phys. Rev. Lett. **80**, 4361 (1998) and references are therein.
- [8] J. Gong and P. Brumer, Phys. Rev. E **60**, 1643 (1999).
- [9] E. Bittner and P. Rossky, J. Chem. Phys. **103**, 8130 (1995).
- [10] O. Prezhdo, Phys. Rev. Lett. **85**, 4413 (2000).
- [11] M. Shapiro and P. Brumer, Adv. At. Mol. Opt. Phys. **42**, 287 (2000).
- [12] M. R. Gallis and G.N. Fleming, Phys. Rev. A 42, 38 (1990); *ibid.* A 43, 5778 (1991).
- [13] N. Gisin and I. Percival, J. Phys. A **25** 5677 (1992) and references are therein.
- [14] M.D. Feit, J. A. Fleck and A. Steiger, J. Comput. Phys. **47**, 412 (1982).
- [15] J. R. Klauder and W. P. Petersen, SIAM J. Numer. Anal. **22**, 1153 (1985).
- [16] B. Liu, J. Chem. Phys. **58**, 1925 (1973); P. Siegbahn and B. Liu, J. Chem. Phys. **68**, 2457 (1978); D. G. Truhlar and C. J. Horowitz, J. Chem. Phys. **68**, 2466 (1978).
- [17] E. A. McCullough, Jr. and R. E. Wyatt, J. Chem. Phys. **54**, 3578 (1971).
- [18] J. M. Bowman and A. Kuppermann, J. Chem. Phys. **59**, 6524 (1973) and references therein.
- [19] H. Lee and T. George, J. Chem. Phys. **84**, 6247 (1986).
- [20] C. C. Rankin and W. H. Miller, J. Chem. Phys. **55**, 3150 (1971).
- [21] Y. Elran and P. Brumer, J. Chem. Phys. **121**, 2673 (2004); Y. Elran, R. Kapral and P. Brumer, (manuscript in preparation).

- [22] H. Han, Ph. D. Dissertation, University of Toronto, (2004).
- [23] S. Mahapatra and N. Sathyamurthy, *J. Chem. Phys.* **105**, 10934 (1996).
- [24] H. Ushiyama and K. Takatsuka, *J. Chem. Phys.* **109**, 9664 (1998).
- [25] W.H. Zurek and J. P. Paz, *Phys. Rev. Lett.* **72**, 2508 (1994); A. R. Kolovsky, *Phys. Rev. Lett.* **76**, 340 (1996); A. R. Kolovsky, *Europhys. Lett.* **27**, 79 (1994).
- [26] Here $\Delta t = 0.002$ for the closed quantum systems in all cases. For SBW, $\Delta t = 0.002/4$ for QMD. For the SBS and DB cases of the higher nonlinearity, $\Delta t = 0.002/16$ for QMD. For the grid size of quantum calculation, $\Delta x = 0.068$ for SBW and $\Delta x = 0.02$ for SBS and DB. The quantity x_0 is chosen so that the initial wavepacket is placed in the asymptotic (force-free) region. In addition, γ is chosen carefully so that for SBW $\delta E \leq 0.01$ and for SBS and DB $\delta E \leq 0.1$, in other words, so that the wavefunctions belonging to different initial energies should not overlap one another since the energy interval of interest is taken as 0.025 for SBW and as 0.2 for SBS and DB.
- [27] R. Liboff, *Quantum Mechanics*, 2nd ed. (Addison-Wesley, Massachusetts, 1992).
- [28] For a thorough discussion of the semiclassical S -matrix approach in molecular collisions, see W. H. Miller, *Adv. Chem. Phys.* **30**, 77 (1975).
- [29] Y. Elran and P. Brumer (work in progress)
- [30] J. P. Paz, S. Habib, and W.H. Zurek, *Phys. Rev. D* **47**, 488 (1993)
- [31] S. A. Rice, *Diffusion-limited Reactions* (Elsevier, Amsterdam, 1985).

FIGURE CAPTIONS

Figure 1. Collinear reactive transition probabilities in $\text{H} + \text{H}_2$ versus the initial total energy E , without and with decoherence. Here $D = 2.47 \times 10^{-35}$ kg·J/s.

Figure 2. As in Fig.1, but with 20 times stronger decoherence, i.e. , $D = 4.94 \times 10^{-34}$ kg·J/s.

Figure 3. Left panel: Potential energy of SBW with scale at left, and the first derivative of SBW with scale at right. For comparison, the much sharper SBS potential energy is shown as well. Right panel: Potential energies and their first derivative for the SBS and DB cases. Thin lines and thick lines correspond to SBS and DB, respectively.

Figure 4. Transmission probabilities as a function of initial energy, E , without and with decoherence. (a) SBW case, (b) SBS case, and (c) DB case. All variables are in dimensionless units.

Figure 5. Time dependence of δE for the open and closed SBS system. Solid lines and cross symbols denote the quantum and classical results, respectively, for the open system; from top to bottom E takes the values 3.0, 2.0 and 1.4. A thick dashed line along $\delta E = 0.1$ denotes the quantum and classical results for the closed system. All variables are in dimensionless units, and all initial $\delta E \approx 0.1$.

Figure 6. Transmission probabilities for the DB case, with and without decoherence, for various masses, to test the predicted D_R [Eq. (26)]. (a) $m = 1$, $t_R=6$, $\delta E_R=0.6$, $D_R = D_2=0.006$, $D_1=0.003$, (b) $m = 2$, $t_R=8$, $\delta E_R=0.5$, $D_R = D_2=0.007$, $D_1=0.002$, (c) $m = 3$, $t_R=9$, $\delta E_R=0.3$, $D_R = D=0.0035$.

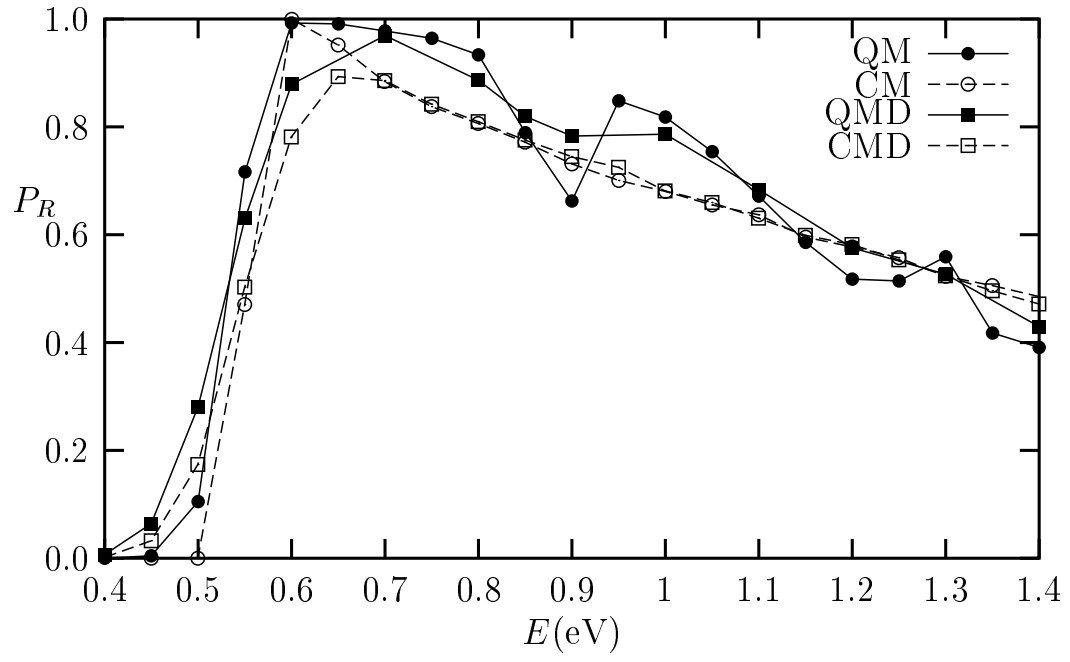


FIG. 1:

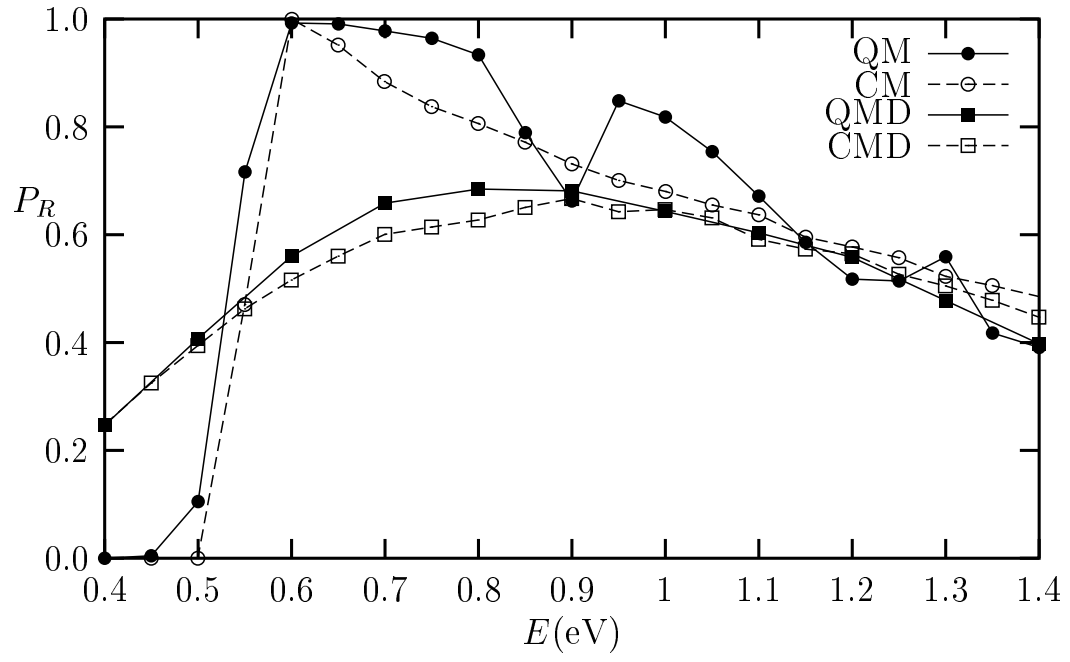


FIG. 2:

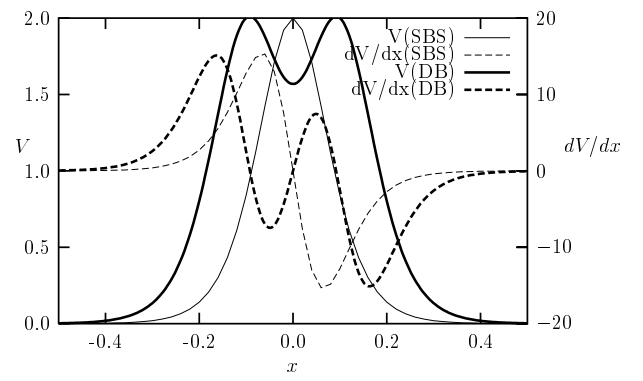
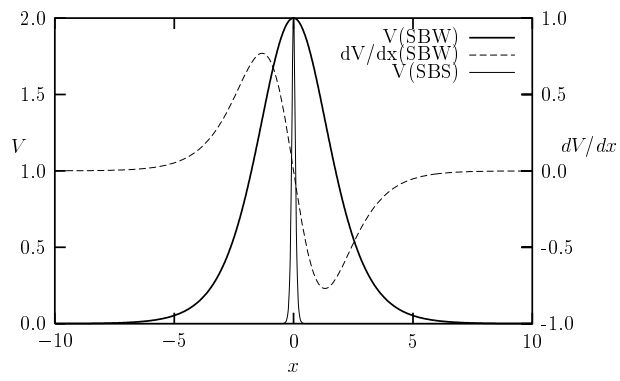


FIG. 3:

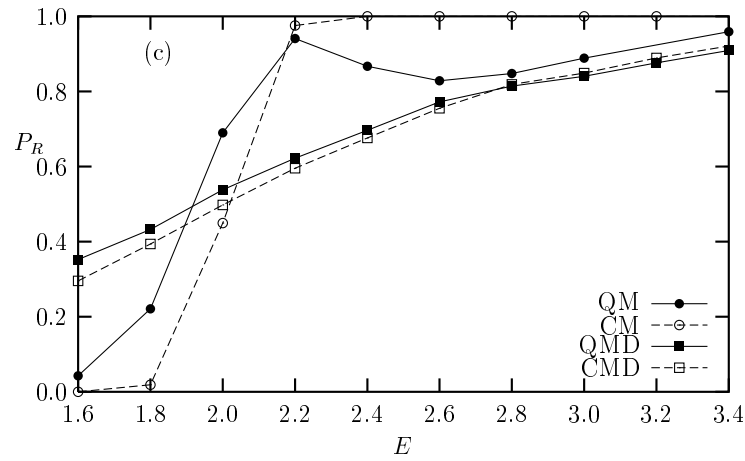
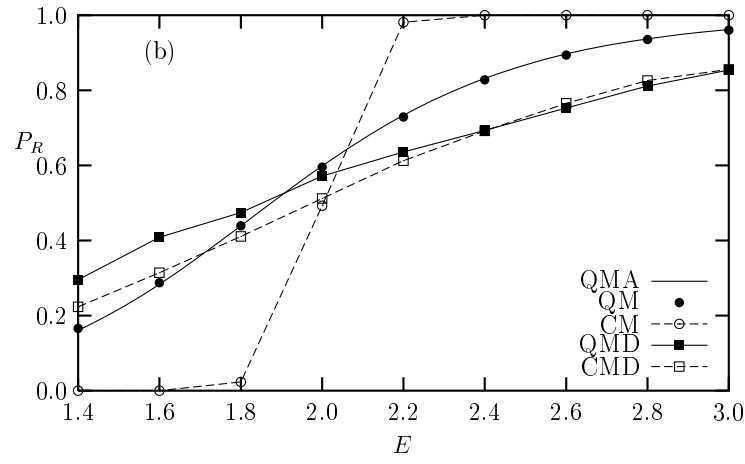
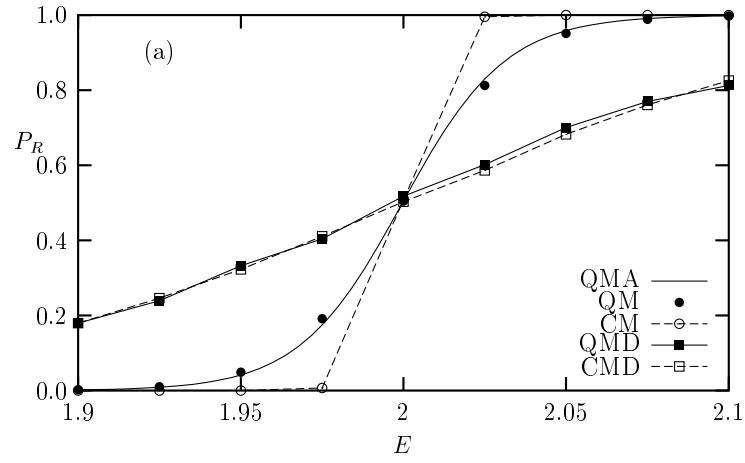


FIG. 4:

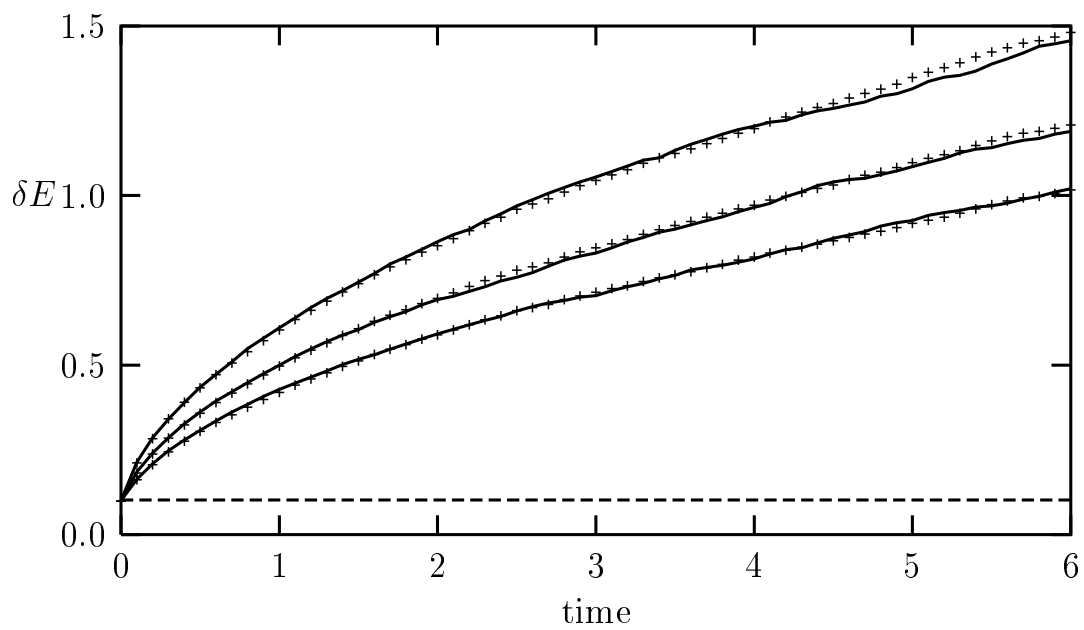


FIG. 5:

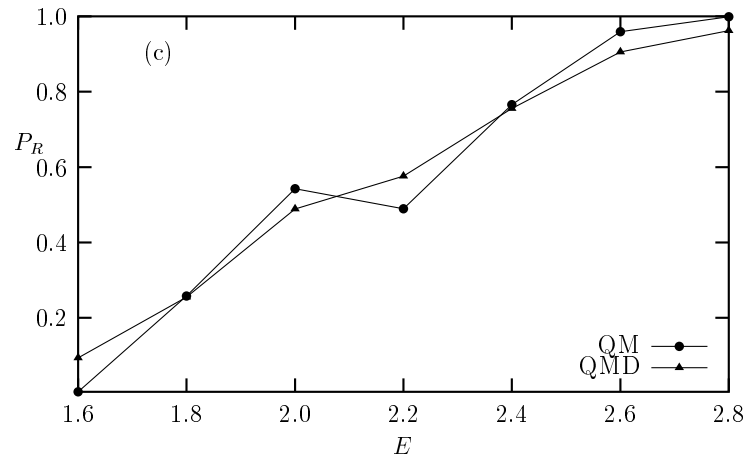
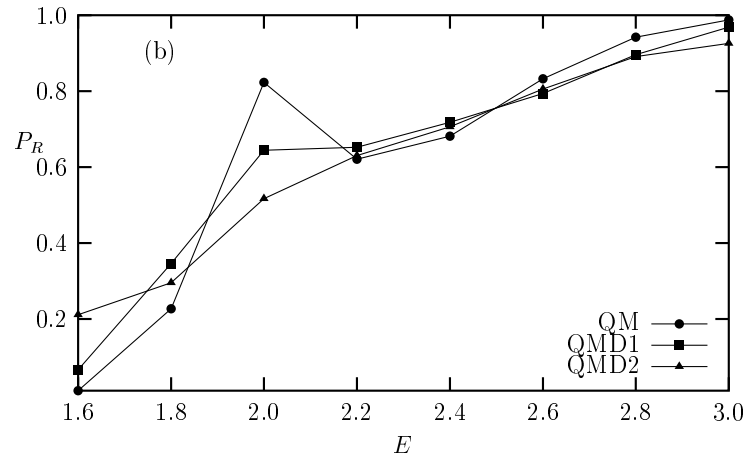
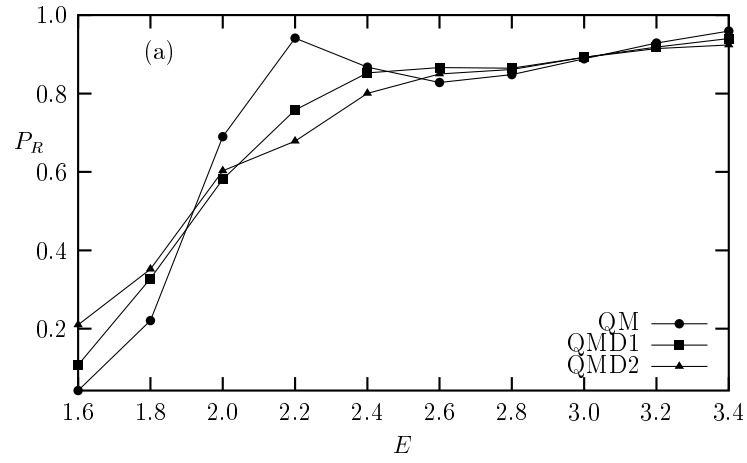


FIG. 6: